Radar based precipitation climatology in central Catalonia

Francesc Roura-Adserias, University of Innsbruck, Austria

February 2022

Abstract

In the present work, a 8 year (2013-2020) radar-based summer precipitation climatology is built in order to study changes in precipitation in an area with sharp contrasts in land use. We have been able to detect higher precipitation amounts in the dry, non irrigated sector than in the wet, irrigated region for July. These differences in precipitation come from the high intensity precipitation episodes.

1 Introduction

Terrain characteristics is a key element that influences the planetary boundary layer. Specifically, the existence of different vegetation types in some cases can lead to a spatial shift of low level convergence lines, convection and ultimately convective precipitation distribution during summer (Huang et al. 2019).

The reason behind it is that regions with less or drier vegetation get warm more rapidly than regions with more or moister vegetation. Part of the incident solar radiation is spent in phase changes (latent heat) so air in drier regions can get warm and more buoyant faster than in moist regions. As a result of this change in buoyancy, if a sharp limit exists between differently vegetated areas, convergence lines and convection are shifted towards the drier sector.

It is important to note that this effect is relevant in periods when the solar incidence and the vegetation contrast is maximum (late spring and summer) as there is more available energy for phase changes and convection.

The present work area of study is located in the Lleida plain, in central Catalonia (NE Iberian Peninsula). Although surrounded by complex topography, the region terrain is fairly flat (terrain slope $< 2\%$) with a sharp contrast in vegetation type, that coincides with the boundary between irrigated and non irrigated zones (Figure 1). The total area of study comprises the non irrigated (dry) region at the east and the irrigated region (wet) at the west, separated by the Urgell channel and encloses a total of $600 km^2$ (30 x 20 km).

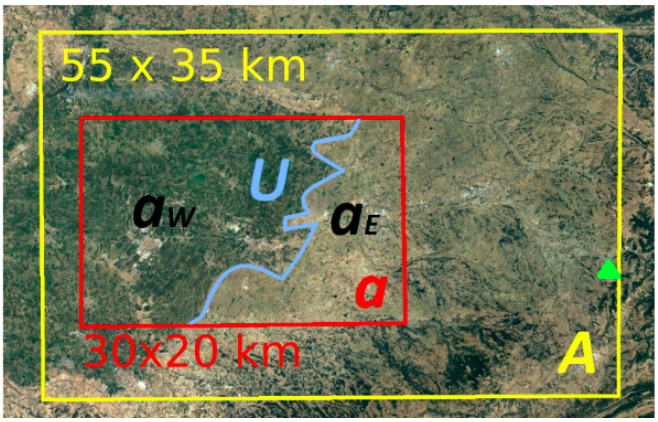

Figure 1: Location of extended area of study A, inner area a, wet and irrigated aW , dry and not irrigated aE and the Urgell channel (U). The green triangle shows the location of the weather radar from the (XRAD) that is located inside our area of study.

In order to study the precipitation regimes, 2013-2020 radar quantitative precipitation estimates (QPE) from the Catalan Meteorological Office (SMC) are used (Trapero et al. 2009). Hourly precipitation estimates allows us to distinguish between convective (high intensity) and stratiform (low, moderate intensity) precipitation and ultimately to obtain the precipitation totals during the events. According to (Huang et al. 2019) we expect higher precipitation amounts in the dry, non irrigated sector than in the wet sector during convective episodes, as convective episodes should be more frequent in the dry sector.

2 Methodology

2.1 Data

We use hourly QPE from the SMC (Trapero et al. 2009). This product is derived from the Radar Network from the SMC (XRAD) corrected with rain gauges from automatic weather stations (XEMA).

XRAD is composed of four C-band doppler, single polarized radars that cover the whole area of Catalonia. A 1x1km resolution Constant Altitude Position Plan Indicator (CAPPI) reflectivity field is converted

to precipitation intensity using the Z-R Marshall-Palmer relation (Marshall and Palmer 1948). The hourly estimates are a combination of the 6-minute radar scanning cycle that takes place during an hour (10 cycles).

After the conversion to hourly precipitation intensity is done, the 2-D precipitation field is validated and corrected using rain gauge data, that is interpolated to the radar 1x1km resolution grid. The final data sets consist of hourly precipitation estimates at 1x1km spatial resolution.

2.2 Intensity dependent mean accumulation

In the present study data from the $600km^2$ area (a) from January 2013 to March 2021 are used. We have computed monthly mean precipitation amounts for each of the 600 grid points, distinguishing between accumulation during low $[0, 3)mmh^{-1}$, moderate $[3, 7.6)mmh^{-1}$ and high $[7.6, \infty)mmh^{-1}$ intensity episodes. The monthly mean for summer months (June, July, August) has been computed as the sum of all hourly accumulations during the period.

Periods with missing files have been tackled using a linear correction K_{corr}, that is, we assume that the periods with no data have the same behaviour as the periods with existing data:

$$PPT_{corrected} = K_{corr} * PPT_{existing} \quad (1)$$

being K_{corr} the ratio between the whole period and the period with data.

2.3 Extended climatology

In order to locate the region of study in its climatic context, we have computed a climatology for an extended region (A), using the same methods and data as used in the smaller region a.

3 Results

Figure 2 shows the precipitation amounts for the extended region during summertime. At north, east and south we find the higher values, peaking at $120mm$ while absolute and relative minima are located in the central, flat terrain, around $60mm$. A non physical out of scale maximum is located at the south eastern corner.

The distribution of precipitation at each subregion a_w and a_e is depicted using precipitation accumulation histograms (Figures 3, 4, 5). The distribution of precipitation amounts is similar for June and August for low, moderate and high intensity episodes

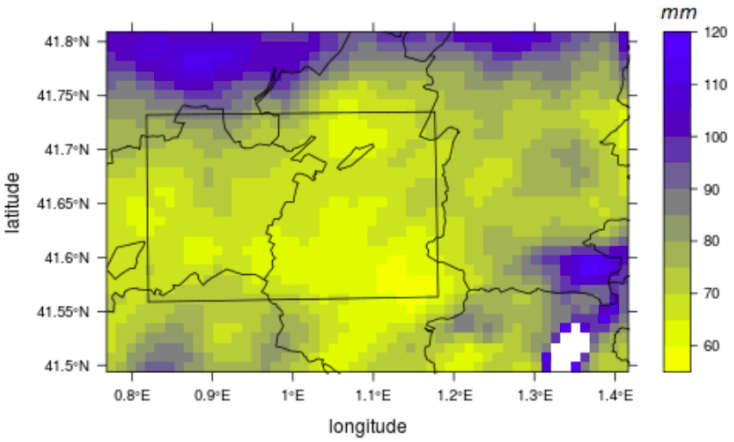

Figure 2: Summer mean precipitation (mm) over the extended region A for the 2013-2020 period. Region a (black rectangle) as well as the administrative regional borders are shown.

as well as for the accumulated summer precipitation (not shown). In contrast, July climatology shows a clear differentiation of precipitation amounts between subregions.

In low intensity episodes (Figure 3), the wet subregion a_w receives more precipitation than the dry one a_e with a mean around 11mm for the former and 9mm for the later. Both distributions are unimodal.

In moderate intensity episodes the distribution in both subregions follow a similar distribution with respect to mean and standard deviation, around 5mm (not shown).

Precipitation during high intensity episodes (Figure 4) displays a different behaviour between subregions. Although both distributions are unimodal, their shape differ notoriously. Not only the distribution differs, but also their mean. While mean precipitation in wet subregion a_w is found around 6mm, the distribution in the dry area a_E averages around 11mm.

Total accumulation follows the same pattern as high precipitation distribution, with wetter eastern, dry subregion (Figure 5).

4 Discussion

Summer climatology shown in Figure 2 agrees with the official climatology from the SMC (Meteocat 2008) although the comparison can only be qualitative as the later spans over the 1960-1990 period. The west-east and plane-mountain gradient can be noticed in both climatologies.

The south-eastern absolute maximum does not affect our main area of interest but it is worth mentioning that it can be attributed to radar beam blocking

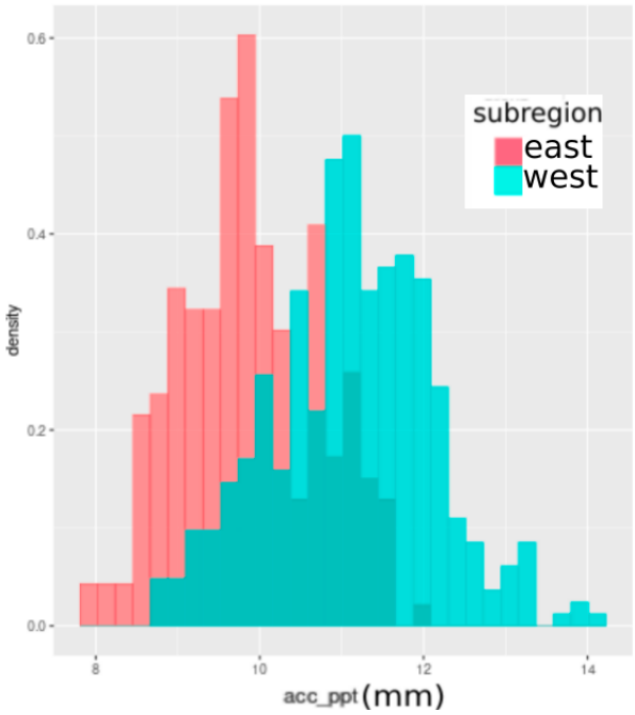

Figure 3: Normalized distribution of the July mean accumulation for low intensity episodes in the 2013-2020 period over aW (irrigated, in blue) and aE (non irrigated, in pink). Overlapping distributions are shown in deeper blue.

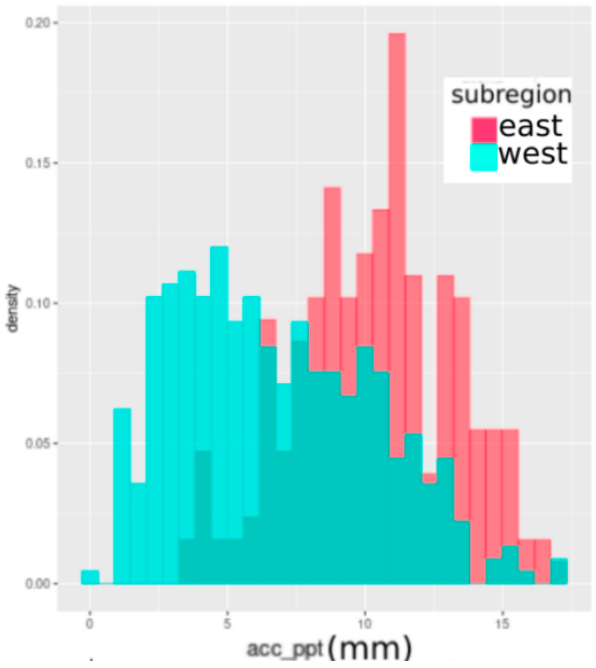

Figure 4: Normalized distribution of the July mean accumulation for high intensity episodes in the 2013-2020 period over aW (irrigated, in blue) and aE (non irrigated, in pink). Overlapping distributions are shown in deeper blue.

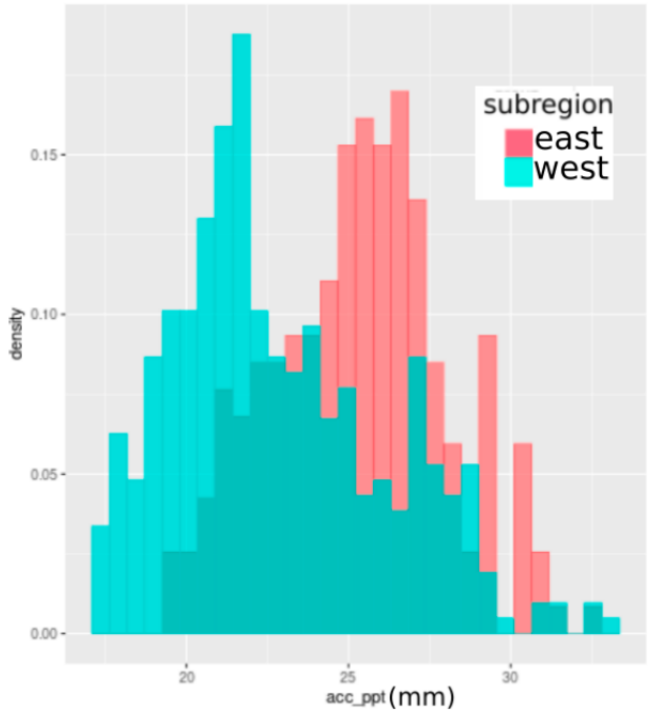

Figure 5: Normalized distribution of the total July mean accumulation in the 2013-2020 period over aW (irrigated, in blue) and aE (non irrigated, in pink). Overlapping distributions are shown in deeper blue.

coming from orography and nearby wind turbines (Argemí et al. 2012). A small but constant signal coming from the blocking is very difficult to correct in an hourly basis and therefore its contribution to the reflectivity (and ultimately precipitation) field is very important when computing long time averages.

Interestingly the enhanced total precipitation accumulation at the dry subregion during July (Figure 5) agrees with our initial hypothesis. Looking at the precipitation accumulations by intensity we can see that this increase in precipitation is associated with the high intensity precipitation episodes. Although we have not performed a low level convergence analysis, we can say that these high intensity episodes are most likely related to convective systems that can be triggered via low level convergence, as stated in (Ge 2008). On the other hand, the wet subregion gets more precipitation during low intensity precipitation events, in agreement with the displacement of the convergence lines (convective precipitation) towards the dry subregion.

Although results for July are promising and agree with our initial hypothesis, August, June and summer average do not present enough signal to support our hypothesis.

4.1 Caveats

This study has some peculiarities that should be taken into account for a complete and rigorous discussion. The first one is that the study has been conducted during summertime, with a very reduced precipitation. Hence this low accumulation totals could be very storm sensitive. In order to overcome this possible issue, we propose a moving window 2-year accumulations analysis. Another weak point is the absence of complementary observations, as other in-situ measurements in addition to the QPE radar product could be very valuable in order to add robustness to our analysis.

5 Conclusions

In the present study we have been able to detect higher precipitation amounts in the dry, non irrigated sector than in the wet, irrigated region for July. These differences in precipitation come from the high intensity precipitation episodes, when locally triggered convective precipitation is assumed to be behind this increase in intensity. However our hypothesis has been proved only partially, as we can not see this pattern during the rest of summer (June and August).

Further studies involving more in-situ data are encouraged to discern local and larger scale precipitation systems.

References

Argemí, O., A. Belmonte, X. , Fabregas, J. Bech, N. Pineda, and T. Rigo, 2012: Wind turbine impact evolution and beam blockage analysis on the doppler weather radar network of the meteorological service of catalonia., URL http://www.meteo.fr/cic/meetings/2012/ERAD/short_abs/NET_013_sh_abs.pdf, the Seventh european conference on radar in meteorology and hydrology.

Ge, Z., 2008: General features of radar-observed boundary layer convergence lines and their associated convection over a sharp vegetation-contrast area. *Ann. Geophys.*, 3819–3829, doi:10.1029/2018GL081714.

Huang, Y., Z. Meng, W. Li, L. Bai, and X. Meng, 2019: General Features of Radar-Observed Boundary Layer Convergence Lines and Their Associated Convection Over a Sharp Vegetation-Contrast Area. *Geophysical Research Letters*, **46 (5)**, 2865–2873, doi:https://doi.org/10.1029/2018GL081714.

Marshall, J. S., and W. M. K. Palmer, 1948: The distribution of raindrops with size. *Journal of Meteorology*, **5**, doi:https://doi.org/10.1175/1520-0469(1948)005⟨0165:TDORWS⟩2.0.CO;2.

Meteocat, 2008: Atles climàtic de catalunya 1961-1990. URL https://www.meteo.cat/climatologia/atles_climatic.

Trapero, L., J. Bech, T. Rigo, N. Pineda, and D. Forcadell, 2009: Uncertainty of precipitation estimates in convective events by the Meteorological Service of Catalonia radar network. *Atmospheric Research*, **93 (1)**, 408–418, doi:https://doi.org/10.1016/j.atmosres.2009.01.021.